ISSN: 2414-1895 DOI: 10.6919/ICJE.202505_11(5).0052

Synthesis of Two-dimensional SnS Nanosheets by Vacuum Thermal Evaporation

Xinyi Lin

School of Physics and Optoelectronic Engineering, Guangdong University of Technology, Guangzhou 510006, China

Abstract

In this paper, two-dimensional SnS nanosheets of different sizes and morphology were synthesised by a facile vacuum thermal evaporation method. We systematically investigated the effects of growth time, evaporation source temperature, substrate temperature and substrate source distance on the size and morphology of nanosheets during the growth process. Two-dimensional SnS nanosheets with a lateral size of about 100 nm were prepared. The results will help to extend and deepen the basic and applied research on SnS two-dimensional materials.

Keywords

SnS; Nanosheet; Vacuum Thermal Evaporation.

1. Introduction

In 2004, André Geim and Konstantin Novoselov pioneered the exploration of two-dimensional (2D) materials with their groundbreaking discovery of graphene, a stable, single-atomic-layer material [1]. Since then, research has expanded to include other 2D materials with intrinsic band gaps, such as hexagonal boron nitride (h-BN) [2], transition metal dichalcogenides (TMDs) [3], group IV metal chalcogenides [4], and black phosphorus (BP) [5]. These materials have demonstrated significant potential in applications ranging from field-effect transistors [6] and photodetectors [7] to gas sensors [8] and flexible electronics [9]. Among emerging 2D materials, layered tin sulfide (SnS) has garnered increasing attention due to its unique properties [10]. Notably, tin is an abundant and cost-effective element in the Earth's crust [11], while SnS is environmentally benign, posing no toxicity risks to humans or ecosystems, aligning with modern demands for sustainable and green technologies [12]. These advantages, combined with its promising electronic characteristics, make 2D layered SnS a highly attractive material for future research and applications [13].

SnS is a group IV-VI layered compound with an orthorhombic crystal structure [14]. First-principles calculations indicate that monolayer SnS exhibits a wider indirect bandgap compared to its bulk counterpart [15]. Various methods have been employed to synthesize 2D SnS nanosheets, including chemical vapor deposition (CVD) [16], liquid-phase exfoliation [17], physical vapor deposition (PVD) [18], and chemical bath deposition [19]. For instance, Higashitarumizu et al. obtained 2D SnS flakes via mechanical exfoliation, achieving a thickness of 3.5 nm and lateral dimensions of 5 μm [20]. Xie et al. employed liquid-phase exfoliation to produce SnS nanosheets with 2-4 atomic layers in thickness, though their lateral size was limited to less than 50 nm [21]. In contrast, Li et al. utilized CVD with Sn and S precursors to synthesize large-area 2D SnS with lateral dimensions up to 330 μm, but the thickness remained substantial at 136 nm [22]. These results suggest that while CVD enables the growth of large-area SnS nanosheets, further optimization is needed to reduce their thickness. Despite significant progress in the synthesis of 2D SnS, achieving a pure-phase monolayer through a simple and scalable method remains a major challenge [23].

ISSN: 2414-1895 DOI: 10.6919/ICJE.202505_11(5).0052

In this work, we synthesized two-dimensional SnS nanosheets via vacuum thermal evaporation and systematically examined the influence of deposition time, evaporation source temperature, substrate temperature, and substrate-source distance on sample growth.

2. Experimental Sectiom

0.05 g of SnS powder (99.95% purity, Alfa Aesar) was weighed into an alumina crucible and placed into one of the evaporation sources of the coater. The cleaned monocrystalline silicon substrate was then fixed on a substrate tray 10 cm above the evaporation source. Subsequently, the chamber door of the coater is closed and a mechanical pump is activated to reduce the pressure in the chamber to 1 Pa. The vacuum is continued by activating a molecular pump until the vacuum level in the chamber reaches approximately 5×10^{-5} Pa. Under these conditions, a temperature ramp-up programme is initiated to heat both the evaporation source and the substrate. After reaching the preset target temperature, the baffle between the evaporation source and the substrate was opened for deposition. After deposition, the baffle and the heating programme are closed and the device is allowed to cool naturally to room temperature. Finally, the vacuum pump system was turned off, the chamber was returned to atmospheric pressure, and the samples were removed for further analysis and characterisation.

3. Structural Characterization and Performance Testing

In order to determine the information about the physical phase, crystallinity and crystal structure of the samples, the samples were tested and characterized by X-ray diffraction (XRD, D8 ADVANCE, Bruker) technique using Cu-Kα diffraction (λ = 1.5406 Å). Morphological features and surface topography were investigated using scanning electron microscopy (SEM, SU8220, Hitachi). At the same time, it is equipped with energy dispersive spectroscopy (EDS) to provide information about the elemental composition of the sample surface.

4. Results and Discussion

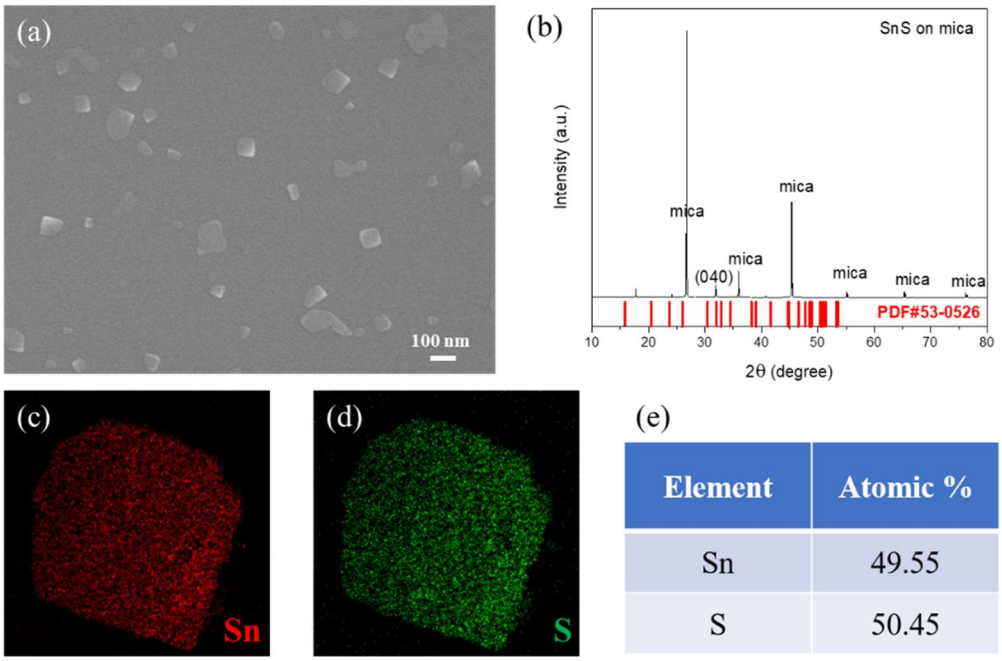

(e)

Element	Atomic %
Sn	49.55
S	50.45

Fig. 1 (a) SEM surface morphology of the sample, (b) XRD spectrum of the sample, (c) Sn and (d) S elemental distribution maps, (e) EDS results within the sample

ISSN: 2414-1895 DOI: 10.6919/ICJE.202505_11(5).0052

Two-dimensional SnS nanostructures were successfully obtained on single-crystal Si substrates via vacuum thermal evaporation. In order to promote the formation of two-dimensional layered growth patterns on the substrate, we controlled the temperatures of the substrate and the evaporation source at 400 °C and 390 °C, respectively. Further, the distance from the evaporation source to the substrate was adjusted to 10 cm, and the deposition time was 5 min to avoid the formation of dense thin film structures on the samples. The morphology and structure of the prepared samples were characterised morphologically and physically, and the results are shown in Fig. 1.

As shown in Fig. 1(a), SEM analysis reveals well-dispersed 2D rectangular nanosheets with lateral dimensions ranging from 50 to 100 nm. The crystalline structure was confirmed by XRD (Fig. 1b), where all diffraction peaks correspond to the orthorhombic SnS phase (PDF#53-0526), exhibiting predominant (040) orientation.As shown in Fig. 1 (c)-(e), EDS elemental mapping demonstrates homogeneous spatial distribution of Sn and S across the nanostructures, with an atomic ratio close to 1:1.

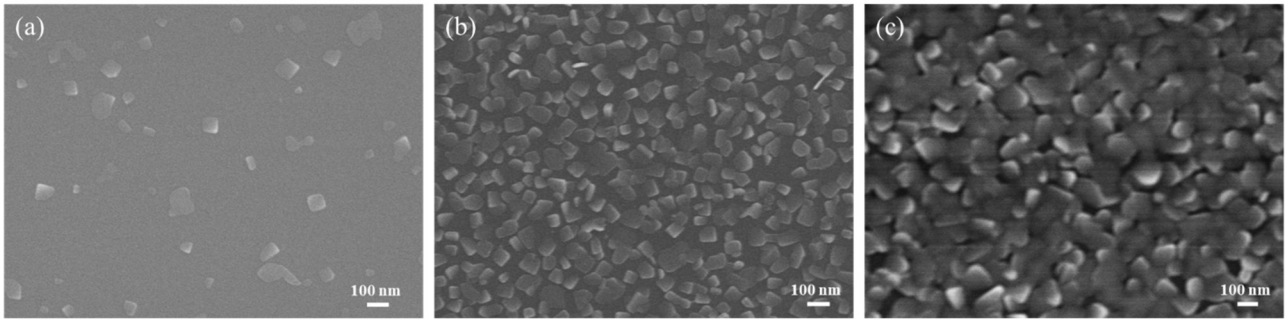

Fig. 2 SEM morphology images of samples with different growth time: (a) 5 min, (b) 10 min, and (c) 15 min

To investigate the effect of growth time on the morphology of 2D SnS structures, we maintained the substrate and evaporation source temperatures at 400 °C and 390 °C, respectively, and set the distance between the substrate and the source at 10 cm, and carried out growth experiments for 5 min, 10 min and 15 min, respectively. The results are shown in Fig. 2. When the growth time is 5 min, the obtained SnS samples mainly exhibit obvious two-dimensional nanosheets, which are sparsely distributed independently of each other, and the number of nanosheets per unit area is relatively small. When the growth time was increased to 10 min, the lateral size of the nanosheets decreased slightly. The number of nanosheets per unit area started to increase, and interconnections between the nanosheets appeared. As the growth time was extended to 15 min, the lateral size of the nanosheets was further reduced, the number of nanosheets per unit area increased significantly, and the interconnections between nanosheets became more obvious, indicating that the samples deposited on the substrate surface were gradually transitioning to denser thin-film structures. These findings establish that prolonged growth irreversibly transitions 2D architectures into quasi-continuous films through vertical stacking-dominated growth, where extended duration promotes nucleation-mediated density elevation rather than lateral expansion, ultimately compromising structural integrity while facilitating layered film formation.

In order to investigate the effect of evaporation temperature on the morphology of the samples, we keep the substrate temperature at 390 °C and vary the evaporation source temperature, and the experimental results are shown in Fig. 3. When the evaporation source temperature is 390 °C, it is observed that the sample consists of small grains interconnected with each other to form a dense film structure. By increasing the evaporation source temperature to 400 °C, the sample was transformed into a nanosheet structure with obvious two-dimensional features. By further increasing the evaporation source temperature to 410 °C, a macroscopic dense film was observed to be formed by the interconnected stacking of dense square grains.

ISSN: 2414-1895 DOI: 10.6919/ICJE.202505_11(5).0052

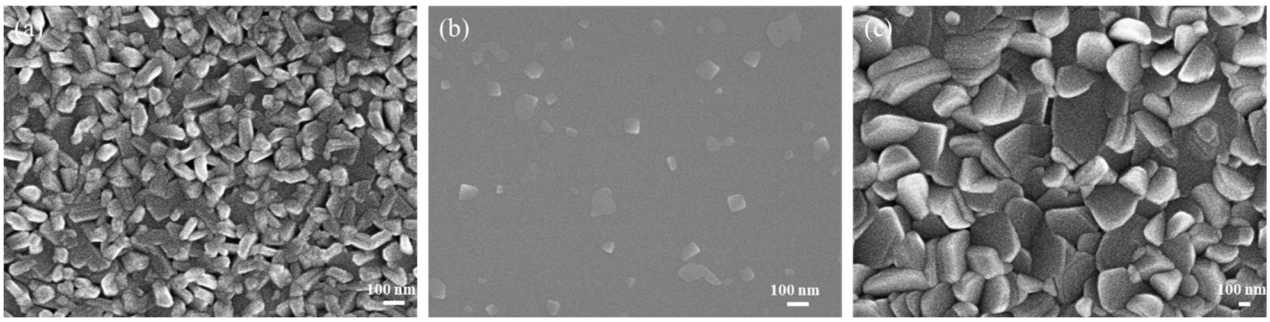

Fig. 3 SEM morphology images of samples with different evaporation source temperatures: (a) 390 °C, (b) 400 °C, and (c) 410 °C

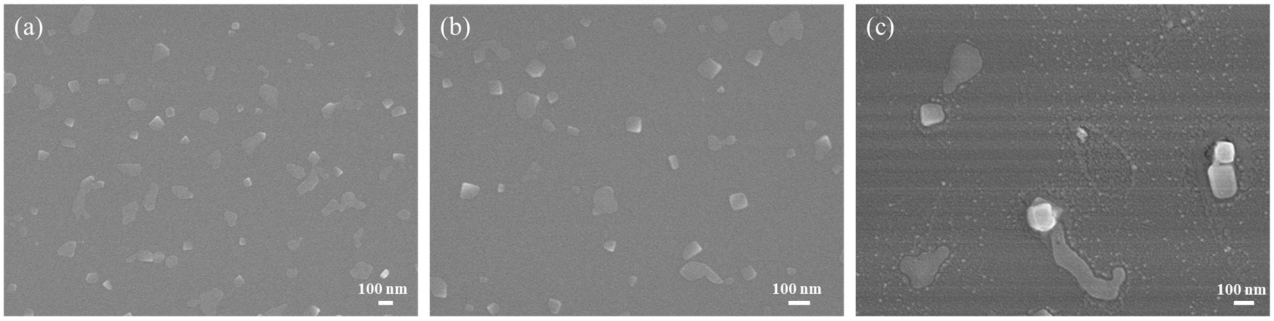

Fig. 4 SEM morphology images of samples with different substrate temperatures: (a) 380 °C, (b) 390 °C, and (c) 400 °C

Systematic investigation of substrate temperature effects reveals thermally driven growth mode transitions as demonstrated in Fig. 4. Under fixed source temperature at 400 °C, increasing substrate temperature from 380 °C to 400 °C induces three sequential growth regimes. At 380 °C, the lateral size of the formed nanosheets is small and the number of nanosheets per unit area is high. As the substrate temperature increases to 390 °C, the lateral size of the nanosheets increases, the number of nanosheets per unit area decreases, and the two-dimensional structure becomes more obvious. When the substrate temperature is further increased to 400 °C, a significant decrease in the number of deposits is observed.

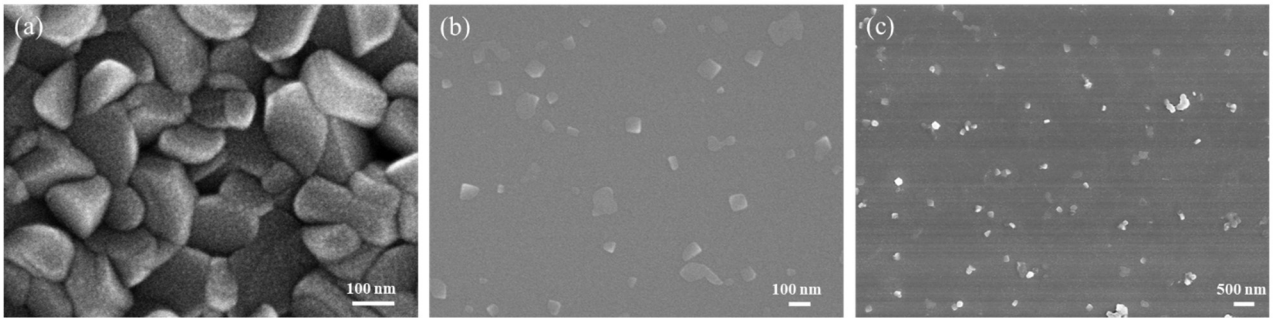

Fig. 5 SEM morphology images of samples with different substrate source distance: (a) 5 cm, (b) 10cm, and (c) 15 cm

In order to clarify how the distance between the substrate and the evaporation source affects the micro-morphology of the samples during the vacuum thermal evaporation process, the experiments were carried out by setting different distances between the substrate and the evaporation source with the evaporation source and substrate temperatures maintained at 400 °C and 390 °C, respectively, and the deposition time set to 5 min. As shown in Fig. 5, reducing the source-substrate distance to 5 cm

ISSN: 2414-1895 DOI: 10.6919/ICJE.202505_11(5).0052

results in densely packed granular structures with an average grain size of 200 nm and high surface roughness. Increasing the distance to 10 cm shifts the growth regime to diffusion-limited conditions, yielding isolated 2D lamellar flakes. By further increasing the liner distance to 15 cm, the sample morphology is observed to be a two-dimensional lamellar structure with smaller sizes, accompanied by the presence of small-sized massive grains.

5. Summary

We have carried out a study on the growth of SnS 2D nanosheets using vacuum thermal evaporation. Growth time governs the transition from discrete nanosheets to vertically stacked films, while optimized source/substrate temperatures (400/390 °C) and source-substrate distance (10 cm) balance nucleation suppression and lateral growth. The maximum lateral size of the samples is about 100 nm. This study provides a scalable route for synthesizing 2D SnS without complex precursors.

References

[1] Novoselov K S, Geim A K, Morozov S V, et al. Electric field effect in atomically thin carbon films. Science. 2004, Vol. 306 (No. 5696), p. 666-669.

[2] Miró P, Audiffred M, Heine T. An atlas of two-dimensional materials. Chemical Society Reviews. 2014, Vol. 43 (No. 18), p. 6537-6554.

[3] Cui Y, Li B, Li J B, et al. Chemical vapor deposition growth of two-dimensional heterojunctions. Science China-Physics Mechanics & Astronomy. 2018, Vol. 61 (No. 1).

[4] De D, Manongdo J, See S, et al. High on/off ratio field effect transistors based on exfoliated crystalline SnS2 nano-membranes. Nanotechnology. 2013, Vol. 24 (No. 2).

[5] Liu H, Neal A T, Zhu Z, et al. Phosphorene: An Unexplored 2D Semiconductor with a High Hole Mobility. Acs Nano. 2014, Vol. 8 (No. 4), p. 4033-4041.

[6] Chang Y R, Nishimura T, Taniguchi T, et al. Performance Enhancement of SnS/h-BN Heterostructure p-Type FET via the Thermodynamically Predicted Surface Oxide Conversion Method. Acs Applied Materials & Interfaces. 2022, Vol. 14 (No. 17), p. 19928-19937.

[7] Modi K H, Pataniya P M, Patel V, et al. Self-powered photodetector functionalized by SnS quantum dots. Optical Materials. 2022, Vol. 129.

[8] Li H, Li M, Kan H, et al. Surface acoustic wave NO2 sensors utilizing colloidal SnS quantum dot thin films. Surface & Coatings Technology. 2019, Vol. 362, p. 78-83.

[9] Shah P R, Pataniya P, Som N N, et al. Flexible and Hand-Printed Photodetector Based on Mg-SnS Nanoflakes. Acs Applied Nano Materials. 2024, Vol. 7 (No. 6), p. 5967-5981.

[10] Qin Y X, Wang J W, Bai Y N. Graphene-Oriented Construction of 2D SnS for Methanol Gas-Sensor Application. Physica Status Solidi a-Applications and Materials Science. 2021, Vol. 218 (No. 6).

[11] Hu Z Y, Ding Y C, Hu X M, et al. Recent progress in 2D group IV-IV monochalcogenides: synthesis, properties and applications. Nanotechnology. 2019, Vol. 30 (No. 25).

[12] Sarkar A S, Stratakis E. Recent Advances in 2D Metal Monochalcogenides. Advanced Science. 2020, Vol. 7 (No. 21).

[13] Yoo C, Adepu V, Han S S, et al. Low-Temperature Centimeter-Scale Growth of Layered 2D SnS for Piezoelectric Kirigami Devices. Acs Nano. 2023, Vol. 17 (No. 20), p. 20680-20688.

[14] Li Z, Su X L, Tang X F. Doping Achieves High Thermoelectric Performance in SnS: A First-Principles Study. Acs Applied Materials & Interfaces. 2022, Vol. 14 (No. 5), p. 6916-6925.

[15] Gomes L C, Carvalho A. Phosphorene analogues: Isoelectronic two-dimensional group-IV monochalcogenides with orthorhombic structure. Physical Review B. 2015, Vol. 92 (No. 8).

[16] Zhang H D, Balaji Y, Mehta A N, et al. Formation mechanism of 2D SnS2 and SnS by chemical vapor deposition using SnCl4 and H2S. Journal of Materials Chemistry C. 2018, Vol. 6 (No. 23), p. 6172-6178.

[17] Brent J R, Lewis D J, Lorenz T, et al. Tin(II) Sulfide (SnS) Nanosheets by Liquid-Phase Exfoliation of Herzenbergite: IV-VI Main Group Two-Dimensional Atomic Crystals. Journal of the American Chemical Society. 2015, Vol. 137 (No. 39), p. 12689-12696.

ISSN: 2414-1895 DOI: 10.6919/ICJE.202505_11(5).0052

[18] Tian Z, Guo C L, Zhao M X, et al. Two-Dimensional SnS: A Phosphorene Analogue with Strong In-Plane Electronic Anisotropy. Acs Nano. 2017, Vol. 11 (No. 2), p. 2219-2226.

[19] Jing J H, Cao M, Wu C S, et al. Chemical bath deposition of SnS nanosheet thin films for FTO/SnS/CdS/Pt photocathode. Journal of Alloys and Compounds. 2017, Vol. 726, p. 720-728.

[20] Higashitarumizu N, Kawamoto H, Nakamura M, et al. Self-passivated ultra-thin SnS layers via mechanical exfoliation and post-oxidation. Nanoscale. 2018, Vol. 10 (No. 47), p. 22474-22483.

[21] Xie Z J, Wang D, Fan T J, et al. Black phosphorus analogue tin sulfide nanosheets: synthesis and application as near-infrared photothermal agents and drug delivery platforms for cancer therapy. Journal of Materials Chemistry B. 2018, Vol. 6 (No. 29).

[22] Li Q, Wei A X, Lu J T, et al. Synthesis of Submillimeter-Scale Single Crystal Stannous Sulfide Nanoplates for Visible and Near-Infrared Photodetectors with Ultrahigh Responsivity. Advanced Electronic Materials. 2018, Vol. 4 (No. 7).

[23] Zi Y, Zhu J, Hu L P, et al. Nanoengineering of Tin Monosulfide (SnS)-Based Structures for Emerging Applications. Small Science. 2022, Vol. 2 (No. 3).